

# Stratification and Mixed Layer Depth around Iceland, characterization and inter-annual variability

Angel Ruiz-Angulo <sup>1\*</sup>, Esther Portela <sup>2</sup>, Charly de Marez<sup>1</sup>, Andreas Macrander<sup>3</sup>,  
Sólveig Rósa Ólafsdóttir<sup>3</sup>, Thomas Meunier <sup>4</sup>, Steingrímur Jónsson <sup>3,5</sup>, and M. Dolores  
Pérez-Hernández <sup>6</sup>

<sup>1</sup>Earth Science Institute, University of Iceland, 101 Reykjavik, Iceland  
<sup>2</sup>Univ. Brest, Laboratoire d'Océanographie Physique et Spatiale, CNRS, IRD, Ifremer, Plouzané, France  
<sup>3</sup>Hafrannsóknastofnun / Marine and Freshwater Research Institute, Hafnarfjörður, Iceland,  
<sup>4</sup>Woods Hole Oceanographic Institution, Woods Hole MA, USA  
<sup>5</sup>University of Akureyri, Akureyri, Iceland  
<sup>6</sup>Unidad océano y clima, Instituto de Oceanografía y Cambio Global, IOCAG, Universidad de Las Palmas de Gran Canaria,  
ULPGC, Unidad Asociada ULPGC-CSIC, Las Palmas de Gran Canaria, Spain  
*Correspondence to:* Angel Ruiz-Angulo (angel@hi.is)

## ABSTRACT

The ocean around Iceland witnesses some of the most important transformations of water masses that drive the global ocean circulation. Here, we analyze 29 years (1990-2019) of quarterly hydrographic ~~section~~ data collected around Iceland. The hydrographic properties around Iceland show important spatial variability. Based on temperature, salinity, and stratification structure, we classified the Icelandic waters in three distinct regions: the South, the North and Northeast regions. The warm and salty Atlantic Waters that dominate the ~~South~~ show the deepest winter mixed layers (~500m) while the North and Northeast show shallower depths (~100m). Based on the decomposition of total stratification into temperature and salinity contributions, we find that, ~~the subsurface stratification is mainly controlled by temperature, in the South, by salinity~~ in the Northwest, while in the North, the North Icelandic Irminger Current and East Icelandic Current alternate ~~seasonally, shifting the region between~~ temperature-dominated and salinity-dominated stratification. The interannual variability of the mixed layer and of its thermohaline properties is also large around Iceland. Mixed layer waters were generally colder in the 90's, then warmed until approximately 2015, and became colder again from 2015 to 2018. In the Northeast, a clear multidecadal mixed layer warming trend clearly emerges from the interannual variability as the Atlantic Water progresses northeastward, which is responsible for transforming locally, the upper stratification from salinity dominated into temperature dominated, allowing for the formation of deeper mixed layers. This is associated with the "Atlantification" of the Arctic. Elsewhere, we observe density-compensated changes in mixed layer temperature and salinity, without clear trends. This study provides an unprecedented and detailed description of the seasonal to multi-decadal variability of the mixed layer depth and stratification around Iceland, ~~showing links between this regional variability and~~ changing North Atlantic under global warming.

**Keywords:** Mixed layer depth, Mixed layer properties, stratification, Ocean warming, Atlantification, Interannual variability

Style Definition: Heading 1: , Hyphenate

Style Definition: Heading 2: , Hyphenate

Style Definition: Heading 3: , Hyphenate

Style Definition: Heading 4: , Hyphenate

Style Definition: Heading 5: , Hyphenate

Style Definition: Heading 6: , Hyphenate

Style Definition: Heading

Style Definition: Body Text

Style Definition: Caption

Style Definition: Index

Style Definition: Comment Text

Style Definition: Revision

Style Definition: Normal (Web)

Style Definition: Footer

Style Definition: Header

Formatted

Deleted: sections

Deleted: south

Deleted: in the South,

Deleted: dominated

Deleted: ,

Deleted: salinity dominates

Deleted: seasonality of the

Formatted: Font colour: Auto

Formatted: Font colour: Auto

Deleted: the

Deleted: contribution to

Formatted: Font colour: Auto

Formatted: Font colour: Auto

Formatted: Font colour: Auto

Deleted: ,

Formatted: Font colour: Auto

Deleted: their link with the

Formatted: Default Paragraph Font, Font colour: Black

Formatted: Normal, Centred, Border: Top: (No border), Bottom: (No border), Left: (No border), Right: (No border), Between : (No border), Tab stops: 7,96 cm, Centred + 15,92 cm, Right, Position: Horizontal: Left, Relative to: Column, Vertical: In line, Relative to: Margin, Wrap Around

Formatted: Font colour: Black

48 1 INTRODUCTION

49 The Nordic Seas, together with the Irminger Sea and the Iceland Basin, play a crucial role on the Atlantic Meridional  
50 Overturning Circulation (AMOC). The Nordic Seas are among the few places on the globe where the formation of deep  
51 waters (1000-3000 m depth) occurs during winter deep convection (Petit et al., 2020). The southern end of the Nordic Seas  
52 is bounded by the Greenland-Iceland-Scotland Ridge (GISR). The North Atlantic Current (NAC) brings the warm and salty  
53 Atlantic Water (AW) northward into the Nordic Seas (Hátún and Chafik, 2018; Østerhus et al., 2019; Hátún et al., 2021).  
54 The AW crosses the ridge in three ways (Fig. 1): (i) between Greenland and Iceland, where the Irminger Current (IC) forms  
55 the North Icelandic Irminger Current (NIIC) bringing AW that flows clockwise around Iceland (Jónsson & Briem, 2003;  
56 Jónsson & Valdimarsson, 2012); (ii) between Iceland and the Faroe Islands (Mauritzen, 1996); and (iii) through the Faroe  
57 Shetland Channel (Hansen and Østerhus, 2000; Hansen et al., 2023), contributing up to 48% of the total AW transport. The  
58 AW undergoes strong cooling and densification in the Nordic Seas and the Arctic Ocean (Våge et al., 2015, 2018; Pérez-  
59 Hernández et al., 2019; Athanase et al., 2020). This modified AW is referred to as Atlantic-origin Overflow Water (AtOW;  
60 e.g., Havik et al., 2017; Casanova-Masjoan et al., 2020) and is one of the two sources of Denmark Strait Overflow Water  
61 (DSOW; Semper et al. 2019). AtOW travels southward as a mid-depth water mass in the East Greenland Current (Håvik et  
62 al., 2017), from where, part of it diverts east and merges with the NIIC northeast of Iceland (Casanova-Masjoan et al.,  
63 2020).

64 The transformation of AW into AtOW takes place in different areas of the Nordic Seas: along the Norwegian Current  
65 (Håvik et al., 2017), in the Iceland Sea Gyre (Våge et al., 2013), on the eastern side of Greenland, or even -due to its  
66 proximity- in the Arctic Basin (Pérez-Hernández et al., 2019). This transformation has different driving mechanisms  
67 impacting mixing and convective processes. Wind-stress and sea-ice retreat drive transformation east of Greenland (Våge  
68 et al., 2018), sea-ice retreat and heat exchange dominate north of Svalbard (Pérez-Hernández et al., 2019; Athanase et al.,  
69 2020), and heat fluxes are the main drivers in the center of Iceland Sea (Våge et al., 2013). Thus, the Nordic Seas region  
70 has been previously described as a “mixing pot” (Renfrew et al., 2019), largely responsible for the overall formation of  
71 deep overflow water (Lozier et al., 2019). The Nordic Seas are also a large repository of freshwater arising from glacier/river  
72 discharge and from the Arctic. This water mass increases buoyancy and is carried southward by the East Greenland Current  
73 (EGC). Therefore, it is crucial to fully understand the variability of the upper ocean, where mixed layers (ML) develop and  
74 transform these water masses.

75 The Arctic Ocean is warming much faster than the global average, a process known as the “Arctic Amplification”, which  
76 is also associated with the “Atlantification” of the Arctic (Polyakov et al., 2017; Dai et al., 2019). Even though the causes  
77 are still in debate, there are evident observed consequences of Arctic Amplification, such as a decrease in the extent of  
78 seasonal sea-ice (Dai et al., 2019) and a weakening of the cold halocline (Polyakov et al., 2020). Changes in temperature  
79 and salinity in the upper ocean modify the upper ocean stratification, which partially controls the mixed layer depth (MLD).

80 The depth and structure of the ML is primarily controlled by local buoyancy forcing, i.e., surface heat loss and freshwater  
81 fluxes, which modifies the water density (Kohler et al., 2018). Wind forcing contributes by enhancing turbulent mixing,  
82 deepening the ML under certain conditions (Petit et al., 2020). For instance, within the Iceland Basin, wintertime buoyancy  
83 loss drives deep convection, shaping the thermohaline properties that influence the lower limb of the AMOC and its  
84 variability in the subpolar North Atlantic (Petit et al., 2021). The pre-existing stratification of the water column is  
85 responsible for controlling the effect of the surface forcing. Strongly stratified upper layers resist mixing, while weak  
86 stratification allows deeper penetration of turbulence and convection mixing (Pierce et al., 1986). Over shorter timescales,  
87 on the order of days, the MLD can significantly deepen as a result of the strong wind events with significant wind stress  
88 and associated large wave heights (Skylvingstad et al., 2023).

Deleted: ridge

Deleted: flowing

Deleted: .)

Deleted: Between

Deleted: .)

Deleted: with

Deleted: western intrusions

Deleted: drives

Deleted: driver on

Deleted: have

Deleted: the

Deleted: the

Deleted: extent

Deleted: to control

Deleted: forcings

Formatted: Default Paragraph Font

Formatted: Default Paragraph Font, Font colour: Black

Formatted: Normal, Centred, Border: Top: (No border), Bottom: (No border), Left: (No border), Right: (No border), Between : (No border), Tab stops: 7,96 cm, Centred + 15,92 cm, Right, Position: Horizontal: Left, Relative to: Column, Vertical: In line, Relative to: Margin, Wrap Around

Formatted: Font colour: Black

104

105 The IPCC report indicates with *high confidence* that roughly 40% of the global ocean mean upper ocean stratification  
106 has increased about 3.3–6.1% since 1960 due to both ocean warming and high latitude freshening (Tessdal et al., 2018;  
107 Yamaguchi and Suga, 2019; Bindoff et al., 2019; Liu et al., 2020; Salleé et al., 2021). Increased stratification is associated  
108 with less efficient *diapycnal* mixing, reducing the exchanges of heat and tracers from the mixed layer into the ocean interior.  
109 It has also been observed, with *high confidence*, that the ML is *undergoing* changes (Bindoff et al., 2019; on Climate  
110 Change, IPCC). Particularly, the shallow summertime ML, which is more likely to be affected by global warming, is  
111 deepening at a rate of 5 – 10 m per decade (Salleé et al., 2021). Despite the reported global patterns, it has been also  
112 acknowledged that regional changes might differ from the global estimates (on Climate Change, IPCC).

Deleted: the

Deleted: undergoing

Formatted: Font: Gungsuh

113 The warming of the ML and the associated increase in stratification influence biogeochemical processes like  
114 phytoplankton blooms and carbon or oxygen sequestration, key components for the Earth’s climate (Olafsson, 2003; Pérez  
115 et al., 2021). In the waters surrounding Iceland, the phytoplankton community is closely linked with the water mass  
116 properties and hence, an “Atlantification” will replace polar communities with more Atlantic communities (Cerfonteyn et  
117 al. 2023). In the Arctic *Ocean*, north and northwest of Iceland, the early onset of stratification in spring gives rise to rapid  
118 shallowing of the mixed layer and triggers early spring phytoplankton blooms, whereas the weakly stratified water-column  
119 in the Atlantic water and associated deep ML delays the spring bloom *South* of Iceland (Zhai et al., 2012). This also has  
120 strong consequences in carbon uptake, vertical nutrient supply and biological processes (Yamaguchi and Suga, 2019).  
121 Other indirect impacts of the increased stratification include changes in upwelling, deep-water formation rates, biological  
122 production, and remineralization rates (Holt et al., 2016), and deoxygenation (Shepherd et al., 2017).

Deleted: south

123 At the regional scale, it is challenging to determine the extent to which changes in stratification and in water-mass  
124 properties are driven by natural or human-induced variability. Moreover, the relatively short observation records in most  
125 of the oceanic regions *hinder* the attribution of the observed changes to the driving mechanisms and forcings. In this study,  
126 by using a long time series of hydrographic observations around Iceland spanning 29 years, we aim at unraveling the  
127 different scales of variability of the water-mass properties, MLD, and stratification around Iceland.

Deleted: hinders

## 128 2 DATA AND METHODS

129

130 We use Conductivity-Temperature-Depth (CTD) data from the repeated hydrographic observational program of the  
131 Icelandic Marine and Freshwater Research Institute between 1990 and 2019. The oceanographic surveys took place  
132 quarterly, mainly in February, May, August, and November with little coverage during the intermediate months.  
133 Observations are made at standard repeated sections. The profiles are obtained with a Seabird 911plus CTD mounted on a  
134 rosette with Niskine bottles. The conductivity data are calibrated with salinity samples taken at the bottom of each station.  
135 All sensors underwent regular calibrations by the manufacturer.

136 In our analyses we considered only the deepest stations in each section (red dots in Fig. 1), including nearby stations  
137 within an area defined by 1° × 0.5° in longitude and latitude (red boxes). The selected stations are located outside of the  
138 Icelandic shelf (about 500 m depth). This criterion was chosen to avoid topographic effects, such as across shelf processes  
139 on the stratification of the water column and to avoid MLDs limited by shallow bathymetry. Thus, the stations in gray, HB  
140 and *JH* in Figure 1 were not considered as they fall on the shelf. For the sake of simplicity these stations will be named  
141 with the acronym of the standard section, first two letters and the station number. The station full name (section and station  
142 number) can be found in Table 1.

Deleted: IB

Formatted: Default Paragraph Font, Font colour: Black

Formatted: Normal, Centred, Border: Top: (No border), Bottom: (No border), Left: (No border), Right: (No border), Between : (No border), Tab stops: 7,96 cm, Centred + 15,92 cm, Right, Position: Horizontal: Left, Relative to: Column, Vertical: In line, Relative to: Margin, Wrap Around

Formatted: Font colour: Black

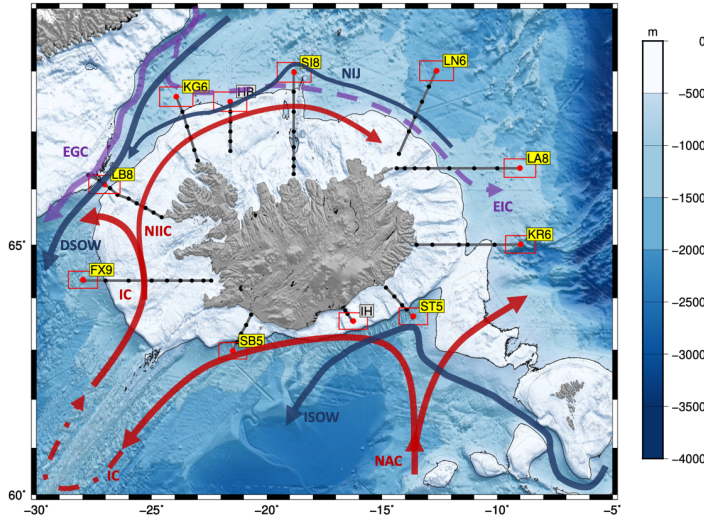


Figure 1: Map of the typical hydrographic sections collected by the Marine and Freshwater Research Institute around Iceland; the black dots represent the nominal location of the standard stations from 1990-2019. The red dots are the stations used for this analysis and the red boxes delimit the area within which all data were considered for this study. The grey bathymetric contours are spaced every 100 m for the shallow water until the 500 m depth (thick black line) and then every 500 m. The hydrographic stations shown in the yellow boxes corresponding to the standard sections: Faxaflói (FX9), Látrabjarg (LB8), Kögur (KG6), Hornbanki (HB), Siglunes (SI8), Langanes NE (LN6), Langanes E (LA8), Krossanes (KR6), Stoksnes (ST5), Ingólfshöfði (IH) and Selvogsbanki (SB5). The gray labeled IH and HB were not used in this analysis. The main surface and deep currents are also depicted on the map.

In this study we analyze the inter-annual variability and linear trends of the ML over a 28-year period as well as the seasonal variability using the seasonal extremes (summer and winter), when there is more data coverage. From the CTD stations we estimated the MLD using the density threshold method with a criterion of  $\rho_{\theta} = 0.01 \text{ kg m}^{-3}$  (as, for instance, in Piron et al., (2016) in the Irminger Sea) and a reference depth of 10 m. We chose this criterion instead of the usual  $0.03 \text{ kg m}^{-3}$  (De Boyer Montegut, 2004) as the latter overestimated the MLD in more than 500 visually inspected profiles (not shown). For comparison and robustness of our chosen method, we also estimated the MLD using other criteria (de Boyer Montegut et al., 2004; Holte et al., 2017). However, we found the density threshold method appropriate for our region as it shows to be effective even for cases where the variations of salinity and temperature were large. Those variations usually compensate in density making this method more suitable. We have validated our method against previous work by Våge et al., 2018, where a glider data was available, and the results were satisfactory.

For each profile we computed the Brunt -Väisälä frequency ( $N^2$ ), defined as:

$$N^2 = g \frac{1}{\rho_{\sigma, \theta}} \frac{\partial \sigma_{\theta}}{\partial z} \quad (1)$$

where  $g$  is the gravity acceleration,  $\rho_{\sigma, \theta}$  is the potential density and  $z$  is depth.  $N^2$  can be decomposed to show the relative contribution of salinity and temperature to the observed stratification as follows:

- Deleted:  $\sigma$
- Formatted: Font: Symbol, Font colour: Black
- Deleted: had a great score
- Formatted: Font colour: Auto
- Deleted:  $\frac{1}{\sigma_{\theta}}$
- Deleted: .
- Deleted: Where
- Deleted:  $\sigma$
- Deleted: on
- Formatted: Default Paragraph Font
- Formatted: Font: Symbol
- Deleted: the
- Formatted: Default Paragraph Font, Font colour: Black
- Formatted: Normal, Centred, Border: Top: (No border), Bottom: (No border), Left: (No border), Right: (No border), Between : (No border), Tab stops: 7,96 cm, Centred + 15,92 cm, Right, Position: Horizontal: Left, Relative to: Column, Vertical: In line, Relative to: Margin, Wrap Around
- Formatted: Font colour: Black

181  $N^2 = N_T^2 + N_S^2$  (2)

Deleted: .

182 where  $N_T^2$  and  $N_S^2$  are the components representing the stratification set by the temperature and salinity, respectively and  
183 are defined as:

Deleted: Where

184  $N_T^2 = g \left( \alpha \frac{\partial T}{\partial z} \right)$  (3)

185  
186  $N_S^2 = g \left( \beta \frac{\partial S}{\partial z} \right)$  (4)

187 where  $\alpha$  is the thermal expansion coefficient and  $\beta$  is the haline contraction coefficient at constant pressure. This  
188 decomposition has also been made to classify the oceans by their stratification contribution into  $\alpha$ -ocean,  $\beta$ -ocean, and  
189 transition zone, where in  $\alpha$ -oceans stratification is permanently dominated by temperature, in  $\beta$ -oceans by salinity and the  
190 transition regions are either intermittently or seasonally dominated by temperature or salinity (Carmack, 2007; Stewart and  
191 Haine, 2016). For the water column to be statically stable,  $N^2$  must be positive. However, the contributions may not be  
192 positive; when any of its components,  $N_T^2$  or  $N_S^2$  are negative, temperature or salinity respectively has a destabilizing effect  
193 on the resulting stratification that must be compensated by the other variable to maintain a stable water column. Small  
194 values of  $N^2$  indicate that the water column is weakly stratified which favors mixing due to winter convection and deeper  
195 MLD.

Deleted: Where

Formatted: Indent: First line: 0 cm

Deleted: have

196 To investigate furthermore the driving mechanism of the MLD we used a one-dimensional model (Price et al., 1986)  
197 initialized with ERA-5 12-hour dataset of wind stress, heat, and freshwater fluxes (Hersbach et al., 2020) and the  
198 summer/winter averaged vertical profiles of temperature and salinity from the observations presented here (see  
199 supplementary material). The 1D model would reveal the contribution from diurnal heating/cooling freshwater fluxes and  
200 wind mixing. In addition, we broaden the impact of our findings by using the hydrographic database published in Brakstad  
201 (2023) that includes, in addition to the dataset from the Marine and Freshwater Research Institute of Iceland, other  
202 multiplatform observations like Argo floats or cruise data between 1950 and 2019. For this objective, a larger oceanic  
203 region is used and classified into  $\alpha$ -ocean and  $\beta$ -ocean using the spice frequency,  $K^2$ , (Carmack, 2007; Strehl et al., 2024),  
204 defined as:

Deleted: .

205  $K^2 = N_T^2 - N_S^2$  (5)

Formatted: Indent: First line: 0 cm

206  $K^2$  is positive (negative) in  $\alpha$ -( $\beta$ -)oceans.

Formatted: Font colour: Auto

Formatted: Indent: Left: 0 cm, First line: 0 cm

## 208 3 RESULTS

### 209 3.1 Hydrographic properties around Iceland

210 The hydrographic properties (potential temperature-salinity diagrams) around Iceland show important spatial, seasonal  
211 and interannual variability are shown in Figure 2; the T/S properties differ widely between the three representative stations:  
212 FX9, SI8 and LN6 for the west, north and northeast of Iceland. FX9, in the southwest of Iceland, is completely dominated  
213 by Atlantic Water (AW; Fig. 2 a and b). At SI8, in the North, the dominating water masses in winter are of polar origin,  
214 i.e., warm Polar Surface Water (PSWw) in the upper layers, and Atlantic Overflow Water (AtOW) and Arctic Overflow  
215 Water (ArOW) in the intermediate/bottom waters (Fig. 2c and d). The SI8 station also presents the largest dispersions of  
216 its thermohaline characteristics. It is noteworthy that using fixed definitions of water masses may lead to biased estimates,  
217 as these water masses have been steadily warming over the past two decades. LN6, in the Northeast, contains the coldest

Formatted: Font colour: Auto

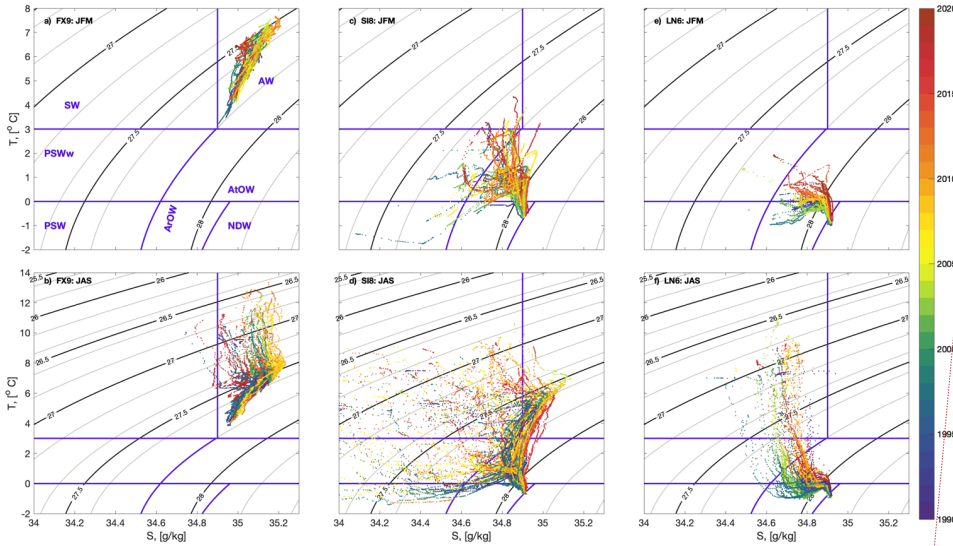
Formatted: Default Paragraph Font, Font colour: Black

Formatted: Normal, Centred, Border: Top: (No border),  
Bottom: (No border), Left: (No border), Right: (No border),  
Between : (No border), Tab stops: 7,96 cm, Centred + 15,92  
cm, Right, Position: Horizontal: Left, Relative to: Column,  
Vertical: In line, Relative to: Margin, Wrap Around

Formatted: Font colour: Black

223 and densest waters on average (Fig. 2c and f).

224



225

226

227

228

**Figure 2: (Top row) Winter (JFM) and (bottom row) summer (JAS) T-S diagrams for three selected stations (a, b) FX9, (c, d) SI8 and (e, f) LN6, considered as representative for the South, North and Northeast regions shown in Fig. 1. The T-S individual profiles are color-coded by year. The main water masses as defined in Table 2, are labeled in panel (a).**

229

230

231

232

233

234

235

The three stations have a clear seasonality. Overall, the summer profiles span a wider temperature range due to seasonal warming of the upper layers (Fig. 2b, d, f) than in winter (Fig. 2a, c, e). FX9 is notably warmer and saltier than the other stations, especially in summer (Fig. 2a), when the minimum temperature in FX9 (nearly 4°C) is as high as the maximum temperature in SI8 and 2 degrees higher than in LN6 (Fig. 2a, b, c). At SI8 a large change in density between seasons is observed mainly driven by the contribution of AW, explained by offshore migration of the NIIC and the stronger inflow of AW during the summer (Fig. 2c, and f) (Jónsson and Valdimarsson, 2012). While the widest seasonal amplitude in salinity is observed at SI8, the largest seasonal amplitude in temperature is observed at LN6.

236

237

238

239

FX9 does not show a clear interannual pattern in summer but in winter the 2000's are strikingly saltier than the other years. In contrast, at SI8 and LN6 fresher and colder waters are observed in the 90's, they progressively warm and become saltier over time, and they reach their maximum temperature and salinity by 2015-2018. This decadal pattern is more evident in winter, but it is observed in both seasons.

240

### 3.2 Seasonality of Stratification and Mixed Layer Depth (MLD)

241

242

243

244

245

The spatial and temporal variability of the stratification around Iceland is remarkably large (Fig. 3 and Fig. 4), and the relative contribution of temperature and salinity shows a strong seasonal cycle. In summer, the MLD is relatively shallow, oscillating around 50 m with a small standard deviation (Fig. 3). In contrast, in winter the ML reaches depths greater than 400 m in FX9, ST5 and SB5 with large standard deviations spanning a 100 m range (Fig. 4). The deepest average MLD is found in FX9 while the shallowest are KG6, SI8, LA8 and KR6.

Deleted:

Formatted: Font colour: Black

Formatted: Font colour: Auto

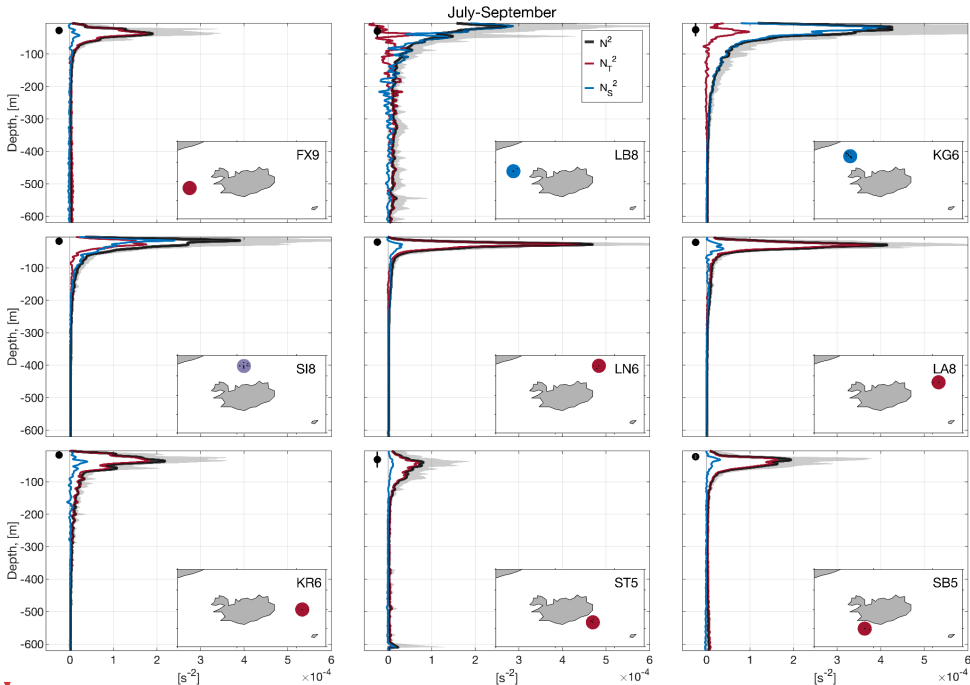
Deleted: strike out as

Formatted: Default Paragraph Font, Font colour: Black

Formatted: Normal, Centred, Border: Top: (No border), Bottom: (No border), Left: (No border), Right: (No border), Between: (No border), Tab stops: 7,96 cm, Centred + 15,92 cm, Right, Position: Horizontal: Left, Relative to: Column, Vertical: In line, Relative to: Margin, Wrap Around

Formatted: Font colour: Black

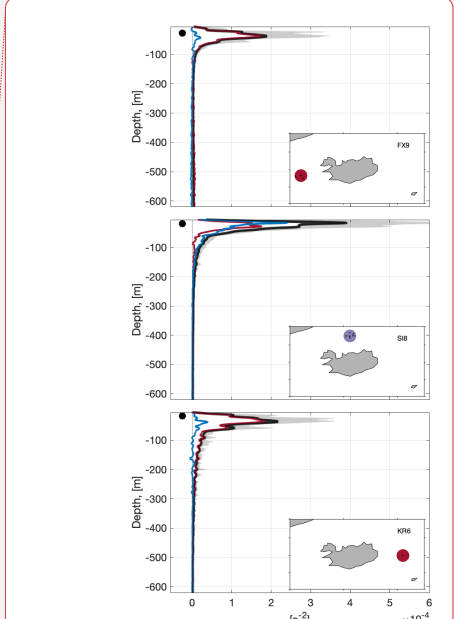
248 In summer (Fig. 3), the upper-ocean stratification around Iceland (Fig. 3) is generally dominated by temperature, except  
 249 for the three Northwestern stations (namely LB8, KG6, SI8). LB8 exhibits the largest variability in both  $N_T^2$  and  $N_S^2$ , but is  
 250 mainly dominated by salinity in the upper 200 m and by temperature below that depth. This transition station is located at  
 251 the sill of Denmark Strait, a convergence zone for several currents (see Table 1 and Fig. 1) carrying water masses with  
 252 contrasting T-S properties within the ML and the thermocline (Jónsson, 1999; Logemann et al., 2013; Casanova-Masjoan  
 253 et al., 2020). In KG6, the fresh inflow from the EGC compensates for the cold temperature, and salinity largely dominates  
 254 stratification. For SI8, we observe a mixed regime with almost equal contributions from both salinity and temperature to  
 255 the total stratification, which suggests that this is also an area of transitional regime. For the stations: LN6, LA8 and KR6,  
 256 despite the fact that stratification is mainly dominated by temperature, exhibits a small subsurface contribution of salinity  
 257 just below the ML, likely due to the presence of fresh PSWw. The southern stations ST5 and SB5, have a minimal  
 258 contribution to stratification from salinity, which may be associated with the numerous river discharges and the proximity  
 259 to the continental shelf. The river discharge is the largest near SB5, likely explaining the summer subsurface contribution  
 260 to salinity (Whitney, 2025).



261 **Figure 3: Summer (JAS) average density stratification ( $N^2$ ) profiles for the selected stations; the average total stratification (black)**  
 262 **is decomposed into temperature (red) and salinity (blue) contributions, while the gray shaded band represents all the stratification**  
 263 **profiles. The black solid dot (left of the profiles) represents the average MLD with the error bar showing the standard deviation as**  
 264 **an indicator of the temporal variability. The maps in the lower corner show the location of the station within a circle color coded by**  
 265 **the dominating regime according to the contribution to stratification: red for temperature, blue for salinity, and purple for a mixed**  
 266 **regime.**

268 The hydrographic conditions are very different for winter; the stratification is one order of magnitude lower, i.e.,  
 269 comparing Figure 3 and Figure 4. Also, the water temperature is much colder due to winter heat loss. Under these  
 270 conditions, the relative contribution of salinity to the total stratification stands out around Iceland except at the southern

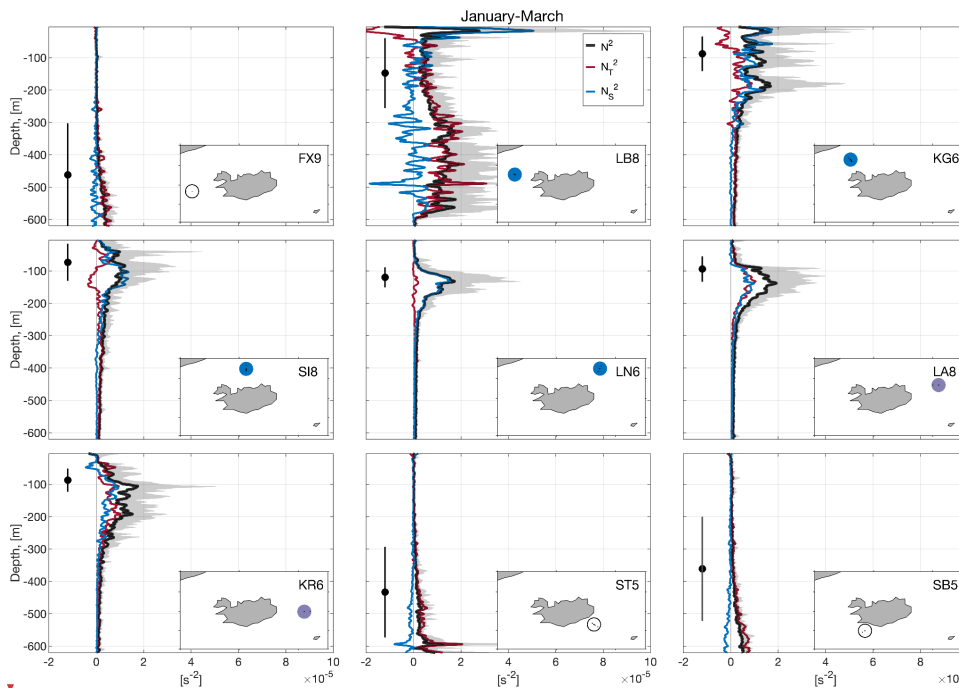
Deleted: due to  
 Deleted: there is  
 Formatted: Font colour: Auto



Deleted:  
 Deleted:  $N^2$   
 Formatted: Font colour: Black  
 Formatted: Font colour: Black  
 Formatted: Font colour: Black  
 Formatted: Font colour: Black  
 Deleted:  
 Deleted: onset is  
 Formatted: Default Paragraph Font, Font colour: Black  
 Formatted: Normal, Centred, Border: Top: (No border), Bottom: (No border), Left: (No border), Right: (No border), Between: (No border), Tab stops: 7,96 cm, Centred + 15,92 cm, Right, Position: Horizontal: Left, Relative to: Column, Vertical: In line, Relative to: Margin, Wrap Around  
 Formatted: Font colour: Black

277 stations (FX9, SB5, ST5), where the weakest winter stratification is observed. This southern region shows the deepest  
 278 MLD, between 350 and 700 m in the stations FX9, SB5 and ST5, while for the northern stations (KG6, SI8, LN6, LA8,  
 279 and KR6) the mean winter MLD is about 100 m. Similar to summer, station LB8, also shows high variability in winter  
 280 stratification, associated with the confluence of currents at the Denmark Strait.

281 The role of temperature or salinity in setting the stratification ( $\alpha$ - and  $\beta$ - ocean, see *e.g.*, Carmack, 2007) is linked to the  
 282 hydrographic characteristics (temperature and salinity) of the dominant water masses within each region. Based on this, we  
 283 can classify the waters around Iceland. The southern side is an  $\alpha$ -ocean as it receives the influence of warm and relatively  
 284 salty AW. Hence, the stratification is mainly temperature driven in both seasons (see FX9, ST5 and SB5 in Figures 3 and  
 285 4) and MLD gets deeper than 400 m in winter. The northwest of Iceland (LB8, KG6) is under the influence of the EGC  
 286 throughout the year bringing fresh PSW and PSWw into the area. Therefore, this area with winter MLDs of 100-150 m can  
 287 be considered a  $\beta$ -ocean, with heat fluxes equivalent to the southern region but with stronger and salinity dominated  
 288 stratification blocking the potential for deep convection, i.e., this region does not have a mechanism to lose surface  
 289 buoyancy seasonally in the salinity component. In contrast, the northeastern Icelandic area (SI8, LN6, LA8 and KR6) shifts  
 290 from  $\beta$  in winter to a mixed  $\alpha/\beta$  in summer. This is likely due to an offshore migration of the NIIC increasing the inflow of  
 291 AW (Jónsson and Valdimarsson, 2012; Casanova-Masjoan et al., 2020, their Figure 11). For instance, in winter, SI8 has a  
 292 PSW signature at the thermocline with salinity driving the stratification and a MLD of about 90 m ( $\beta$ -ocean), and in summer,  
 293 the NIIC brings warm AW to the upper layers of SI8 making the stratification similarly driven by temperature and salinity.  
 294 Overall, the north of Iceland exhibits the strongest summer stratification of the study area which results in very shallow  
 295 MLDs.



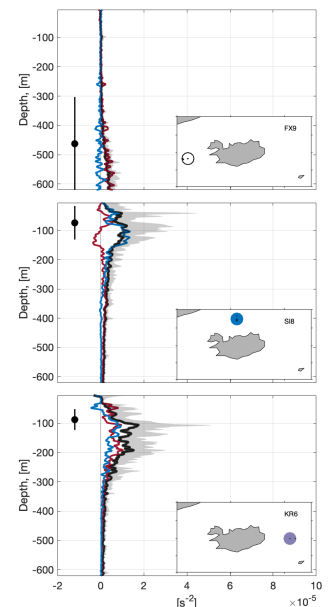
296 **Figure 4: Same as Figure 3 but for winter (JFM). The white color circles shown in the maps of stations ST5, SB5, and FX9 indicate,**  
 297 **very weak winter stratification with no significant contribution of salinity or temperature.**  
 298

Deleted: and

Formatted: Font colour: Auto

Deleted: of

Formatted: Font colour: Auto



Deleted:

Deleted: maps

Deleted: lower corner with a white circle indicates

Formatted: Font colour: Black

Formatted: Font colour: Black

Formatted: Font colour: Black

Formatted: Font colour: Auto

Formatted: Font colour: Black

Formatted: Default Paragraph Font, Font colour: Black

Formatted: Normal, Centred, Border: Top: (No border),  
 Bottom: (No border), Left: (No border), Right: (No border),  
 Between : (No border), Tab stops: 7,96 cm, Centred + 15,92  
 cm, Right, Position: Horizontal: Left, Relative to: Column,  
 Vertical: In line, Relative to: Margin, Wrap Around

Formatted: Font colour: Black

304

### 305 3.3 Interannual to decadal variability of the mixed layer properties

306 To investigate the interannual to decadal ML variability we focused on three reference stations, considered representative  
307 of the  $\alpha$ -ocean (FX9, West), transition (SI8, North) and  $\beta$ -ocean (LB8, Northwest) regimes around Iceland. FX9 dominated  
308 by relatively warm and salty AW, SI8 as a transition area, and LB8 dominated by cold and fresh PSW. The three stations  
309 show strong interannual variability.

310 In FX9, to the West of Iceland, there is a correlation ( $R=0.69$   $p\text{-value}<0.01$ ) between mixed layer temperature (MLT)  
311 and salinity (MLS) anomalies. Between 1990 and 1998 the mixed layer was the deepest, coldest and second fresher period,  
312 as shown in Figure 5a, and d (positive MLD anomalies correspond to deeper ML and negative ones correspond to shallower  
313 ML). Around the period 2000-2014, there is an increase in MLT and MLS as the ML becomes moderate shallower. The  
314 winter MLD is the shallowest, saltiest, and warmest in 2010 (Fig. 5a, and d), where the temperature contribution seems to  
315 control this minimum. From 2015 to 2018 the ML returns to the cold and fresh conditions of the 90's but the MLD is  
316 average. The observed variability of the ML and its temperature in FX9 exhibits certain correlation (R) with the NAO; for  
317 MLD, the best correlation was  $R=0.53$ ,  $p\text{-value}<0.01$  at lag zero; for MLS  $R=-0.52$ ,  $p\text{-value}<0.01$  at lag -2 years (NAO  
318 leading), and for MLT  $R=-0.49$ ,  $p\text{-value}<0.01$  at lag -1 year (NAO leading (Fig. 5g, h). However, we consider that a 2-year  
319 lag lacks a realistic physical explanation, thus, we prefer to not to consider this as a reliable correlation. More qualitatively,  
320 positive NAO at the beginning and the end of the time series, corresponds with deeper colder and fresher MLs, while  
321 negative NAO between 2000 and 2015 roughly corresponds with shallower, warmer, and saltier MLs. As shown in Figure  
322 2, FX9 contains only AW (Fig. 2a, d) likely advected from the South to the area by the Gulf Stream and later the Irminger  
323 Current. Similar conditions have been observed in the Irminger Sea over the same period, and they have been related to the  
324 NAO phase and its impact on the Subpolar gyre (Feucher et al., 2022). This suggests that the FX region is largely influenced  
325 by the Atlantic climate and therefore it is partly impacted by the NAO (Bersch, 2002).

326 At SI8, in the North of Iceland (Fig. 5b, e, h), the negative winter MLD anomalies are on the order of those at FX9 and  
327 also exhibit strong interannual variability without an identifiable pattern. Strong positive MLD anomalies are observed in  
328 particular years (e.g., 2000, 2007, and 2016) but they do not seem correlated with the MLT/MLS or with the NAO  
329 variability. Interestingly, the MLT and MLS co-vary during the period 1990-2005, when the mixed layer is colder and  
330 fresher, but this correlation weakens from 2005 to 2018, when the positive MLT anomalies increase while the MLS  
331 anomalies, although positive, do not vary significantly.

332 In LB8 (Northwest), the winter MLD has the largest variability as the station is located in the vicinity of the front between  
333 NIIC and the EGC, which shapes the Polar and Atlantic conditions. Despite this large variability, a co-variance between  
334 MLT and MLS anomalies seems to be correlated with the position of the front. Fresher and colder MLs are associated with  
335 EGC influence and warmer/saltier MLs with the presence of NIIC (Fig. 5c, f, l). Generally, shallower MLs are also fresher  
336 and colder, which agrees with a salinity-dominated stratification in the upper layer (Fig. 4b). Three particular years present  
337 relatively deep, cold, and salty MLs: 1996, 2006 and 2014. The observed interannual variability in the ML and its properties,  
338 while large, does not seem to be correlated with the NAO, except the last decade where the high state of the NAO is  
339 consistent with the positive MLT and MLS, suggesting a larger presence of the NIIC at this station.

Deleted: for an  $\alpha$ -ocean

Deleted: for a  $\beta$ -ocean

Deleted: high

Deleted: shows a

Deleted: shallowing

Deleted: properties in FX9 correlates with the NAO (Fig. 5g, h). Positive

Deleted: south

Deleted: in

Deleted: exhibits

Deleted: neither

Deleted: nor

Deleted: it

Formatted: Font colour: Auto

Deleted: , fresher

Formatted: Default Paragraph Font, Font colour: Black

Formatted: Normal, Centred, Border: Top: (No border), Bottom: (No border), Left: (No border), Right: (No border), Between : (No border), Tab stops: 7,96 cm, Centred + 15,92 cm. Right, Position: Horizontal: Left, Relative to: Column, Vertical: In line, Relative to: Margin, Wrap Around

Formatted: Font colour: Black

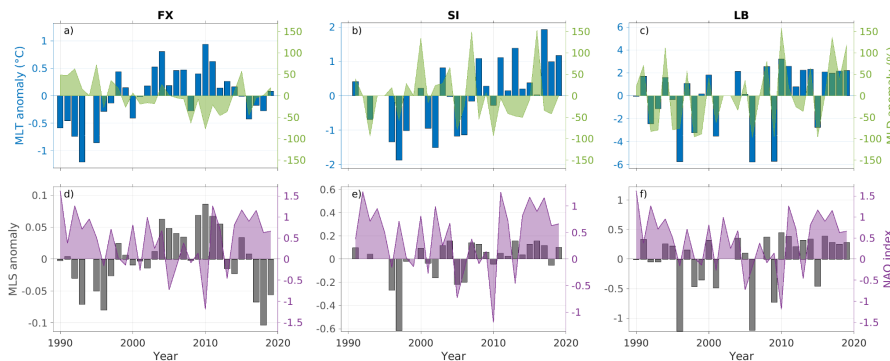
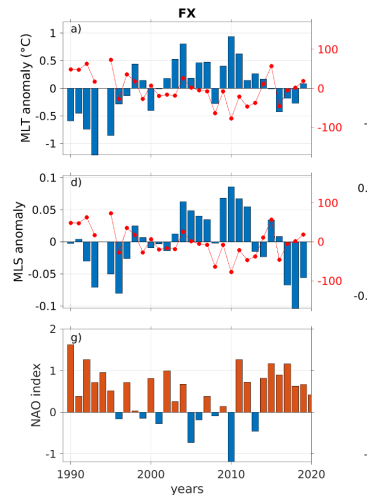


**Figure 5: Interannual winter (JFM) variability from 1990 to 2018 in three stations representative of different regions around Iceland, of: (a, b, c) MLD anomaly (in percentage of its mean winter value over the whole record, green shading) and mixed layer temperature (MLT, blue bars). (d, e, f) Mixed layer salinity (MLS, grey bars) and winter average NAO index for comparison (purple shading). The represented stations are (a, d) FX, in the Southwest, (b, e) SI, in the North, and (c, f) LB in the Northwest. Positive anomalies in MLD, MLS and MLT correspond to deeper, warmer and saltier waters, respectively. The summary of the correlations is presented in Table 1.**

*Table 1: Pearson correlations between different variables. Non significant correlations have been omitted. The shown correlations are significant at 95% confidence ( $p < 0.05$ ), and those significant at 99% ( $p < 0.01$ ) are in bold.*

	FX		SI		LB	
	Correlation	p-value	Correlation	p-value	Correlation	p-value
MLT-MLS	<b>R=0.69</b>	<b>P&lt;0.01</b>	<b>R=0.74</b>	<b>P=&lt;0.01</b>	<b>R=0.95</b>	<b>P&lt;0.01</b>
MLT-MLD	-	-	-	-	<b>R=0.76</b>	<b>P&lt;0.01</b>
MLS-MLD	-	-	-	-	<b>R=0.68</b>	<b>P=&lt;0.01</b>
NAO-MLD	<b>R=0.53</b>	<b>P&lt;0.01</b>	-	-	-	-
NAO-MLT	R=-0.41	P<0.03	-	-	-	-
NAO-MLS	-	-	-	-	-	-

To delve into the interannual to decadal variability of the MLT around Iceland, we analyzed its anomalies (relative to the long record) in all nine stations and computed their linear trends (Fig. 6). The temperature anomalies show significant interannual variability and spatial differences around Iceland. For instance, positive anomalies were observed in 2003 in most of the stations in both seasons, with particularly large temperature anomalies east of Iceland. Strong warm anomalies are also observed in 2017, mostly in summer at all stations except FX9 and SB5, located South of Iceland (Fig. 6; left panel). Although the 28-years period might be too short for identifying linear anthropogenically-driven trends, linear trends are significant in some of the stations, (where the p-value is indicated). The linear trends show a general warming of the mixed layer that is more evident in winter, mainly in the stations of the northeast (LN6, LA8). In the South (ST5, SB5 and FX9), even if the trend is significant from 2000-2015, there is an interannual variability that induces colder mixed layer



Deleted:

Deleted: of the MLD anomaly with negative values associated with shallower MLs (red line), its temperature (MLT, first row) and its salinity (MLS, second row)

Formatted: Font colour: Black

Formatted: Font colour: Auto

Deleted: The last row (g-i) shows the winter average of the NAO index for comparison. For MLD positive

Formatted: Font colour: Black

Formatted: Font colour: Black

Deleted: ML, positive anomalies in MLT and MLS correspond to...

Deleted: water

Formatted: Font colour: Black

Formatted: Font colour: Black

Formatted: Font colour: Black

Formatted: Font colour: Black

Deleted: arc

Deleted: south

Deleted: south

Deleted: a

Deleted: appears

Deleted: they seem to be aliased with

Formatted: Default Paragraph Font, Font colour: Black

Formatted: Normal, Centred, Border: Top: (No border), Bottom: (No border), Left: (No border), Right: (No border), Between: (No border), Tab stops: 7,96 cm, Centred + 15,92 cm, Right, Position: Horizontal: Left, Relative to: Column, Vertical: In line, Relative to: Margin, Wrap Around

Formatted: Font colour: Black

conditions from 2015 to 2018. This tendency of returning to the conditions observed in the early 90's may be associated with the NAO (Future et al., 2022) as shown in Fig. 5. The observed general warming of the ML around Iceland is consistent with the progressive warming of the NIIC (Casanova-Masjoan et al. 2020).

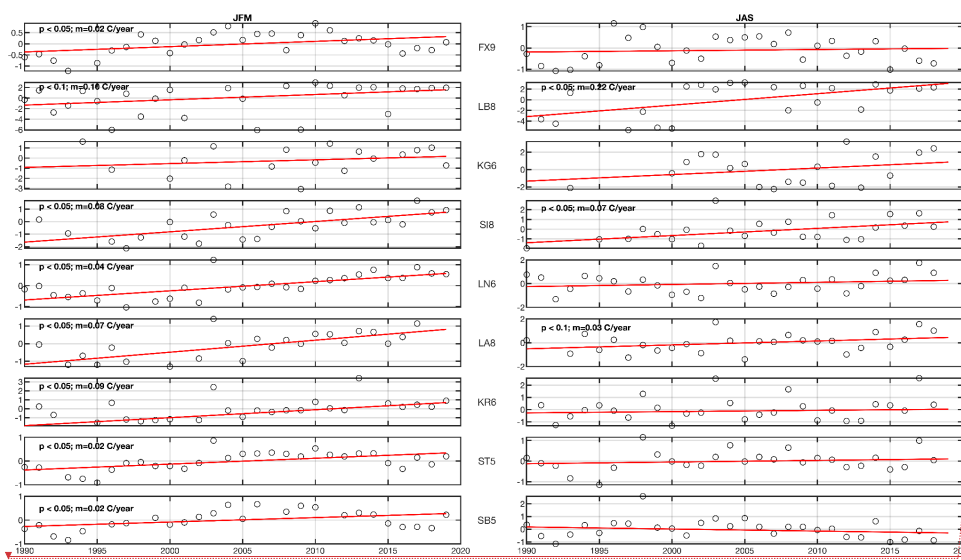


Figure 6: Mixed Layer Temperature (MLT) anomaly time series (left) winter (JFM) and (right) summer (JAS) for the 9 stations shown in Figures 3, 4. The anomalies show the p-values and the linear trends.

#### 4. MLD driving mechanisms from a 1D model

The summer stratification around Iceland is an order of magnitude higher than in winter and hence summer MLDs are very shallow and with higher variability. Therefore, we only use the winter season to study the atmospheric effect on these  $\alpha$ - and  $\beta$ -ocean regions by using the Price et al. (1986) one-dimensional model. It is worth mentioning that the 1D model estimates the MLD from temperature-based profiles while the estimates from observations are density threshold based. The MLDs shown in Figure 7 are within the range of the observed average  $\pm$  standard deviations (black dots and lines in Figure 7). For all stations a spring shoaling of the MLD is driven by heat flux, while the MLD remains relatively deep due to the wind-stress. The choice of PWP model was made to support the idea that  $\beta$ - and transition oceans do not develop deep mixed layers, which is shown in Figure 7.

In the model, the stations embedded in AW (SB5 and ST5) present the largest MLDs exceeding 300 m depth, which is consistent with the observations. In this  $\alpha$ -ocean region, the development of a deep ML is driven mainly by heat fluxes (Fig. 7 h and i), which also holds for FX9. However, wind-stress steadily contributes to the development of the ML (Fig. 7a, h and i). During the summer, shoaling of the mixed layer is likely influenced by the changes of both heat and freshwater fluxes, with their effects on the MLD partially offset by wind stress (Fig. 7a, h and i).

The station LB8, despite being in Denmark Strait and presenting a large contribution of PSWw and PSW in the upper layers (driving a  $\beta$ -ocean stratification), shows that the development of MLDs can be influenced by both, heat flux and/or

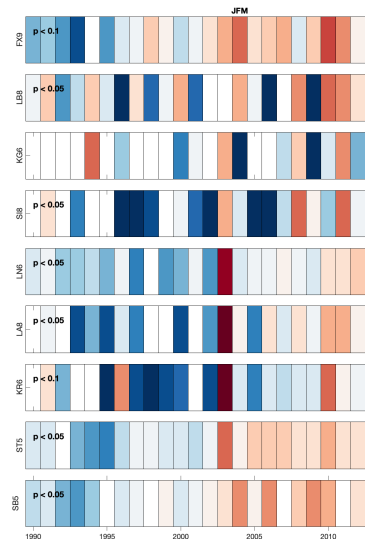
Deleted: return

Deleted: could

Deleted: , Polyakov et al. 2017

Formatted: Font colour: Auto

Formatted: Font colour: Auto



Deleted:

Formatted: Font colour: Black

Deleted: for all stations except LG8

Deleted: KG6 have fixed scale from -1.5 to 1.5 C

Formatted: Font colour: Auto

Formatted: Font colour: Auto

Formatted: Font colour: Black

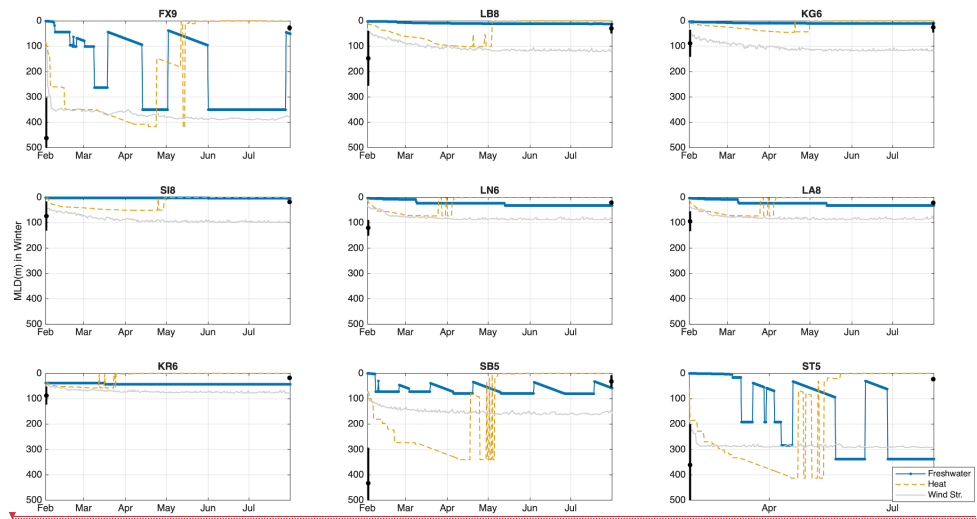
Formatted: Default Paragraph Font, Font colour: Black

Formatted: Normal, Centred, Border: Top: (No border), Bottom: (No border), Left: (No border), Right: (No border), Between: (No border), Tab stops: 7,96 cm, Centred + 15,92 cm, Right, Position: Horizontal: Left, Relative to: Column, Vertical: In line, Relative to: Margin, Wrap Around

Formatted: Font colour: Black

419 wind stress (Fig. 7b). However, the contribution of wind-stress leads to a slightly deeper MLD than the heat fluxes (Fig.  
 420 7b). Wind stress becomes the lead forcing mechanism northeast of LB8 (KG6, SI8), coinciding with the shift from  $\alpha$ - to  $\beta$ -  
 421 ocean stratification (Fig. 7b, c and d). This region represented by LB8 station does not have a large convection potential  
 422 compared to those with pure AW and hence do not produce large MLDs (Fig. 4) and **the MLD is a result of convection**  
 423 **wind-mixing in roughly equal parts.**

424 At LN6, LA8 and KR6 before spring, wind-stress and heat fluxes contribute similarly to the development of the MLD;  
 425 those stations are at the core of the EIC, which contains PSWw in the upper layers and AtOW beneath. Hence the wind-  
 426 stress and heat fluxes are the driving mechanisms acting on the water column (Fig. 7e and f). As the wind-stress develops,  
 427 the MLD evolution erodes the PSWw strata reaching the AtOW layer, allowing the heat fluxes to lead the MLD  
 428 development.



429 **Figure 7: MLD driving mechanism decomposition estimated from the PWP 1-D model (Price et al. 1986) for each of the studied**  
 430 **stations. Different MLD evolutions are shown for outputs forced with freshwater fluxes (blue), heat fluxes (red), and wind-stress**  
 431 **(green). Black dots represent the averaged winter and summer MLD with their standard deviations.**

433 **5. Stratification around Iceland**

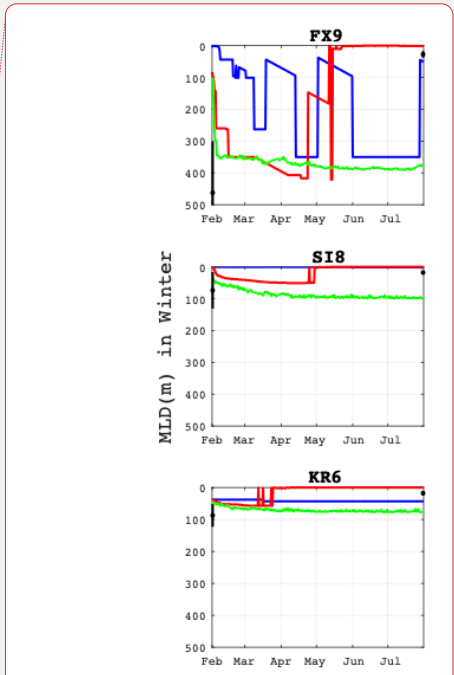
434 To complement the understanding of the stratification of the Arctic and Subarctic waters around Iceland, their connection  
 435 with water masses, currents, and their variability, we used the spice frequency averaged in the first 200 m, estimated  
 436 following the methods described in Strehl et al. (2024) implementing Equation (5). For this analysis we used the  
 437 hydrographic dataset in Brakstad et al (2023). The distribution shown in Figure 8 clearly reveals a southern (northern) side  
 438 where the temperature (salinity) dominates the spiciness and hence marking clear  $\alpha$ -ocean regimes, while the northern part  
 439 has salinity dominated regions associated with  $\beta$ -ocean. These areas largely correspond with the distribution of AW versus  
 440 PSW/PSWw (See Fig. 2 for T-S definitions).

Deleted: ,

Deleted: is mainly driven by

Deleted: stress

Deleted: ,



Deleted:

Formatted: Font colour: Black

Deleted: )

Deleted: (Fig.

Deleted: )

Formatted: Font colour: Auto

Deleted: ( $\beta$ -)

Formatted: Font colour: Auto

Formatted: Default Paragraph Font, Font colour: Black

Formatted: Normal, Centred, Border: Top: (No border), Bottom: (No border), Left: (No border), Right: (No border), Between : (No border), Tab stops: 7,96 cm, Centred + 15,92 cm, Right, Position: Horizontal: Left, Relative to: Column, Vertical: In line, Relative to: Margin, Wrap Around

Formatted: Font colour: Black

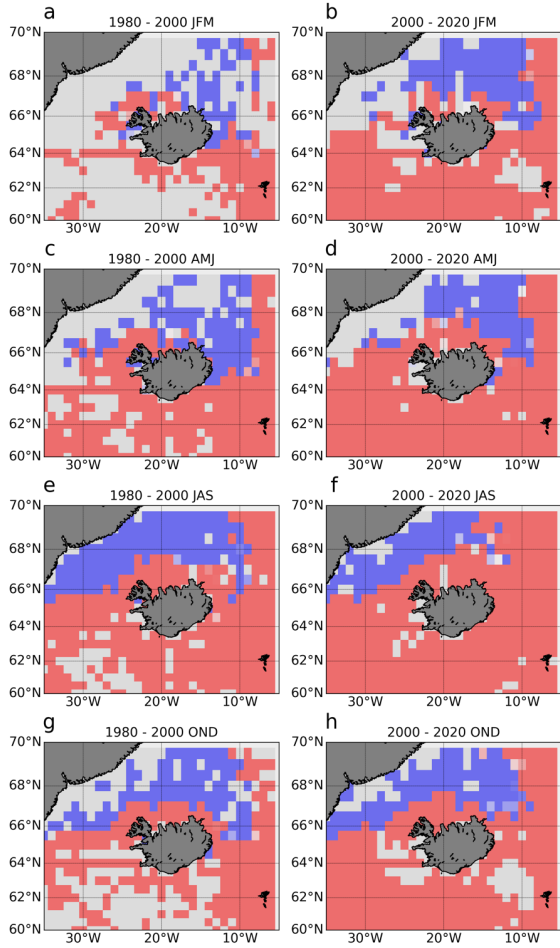
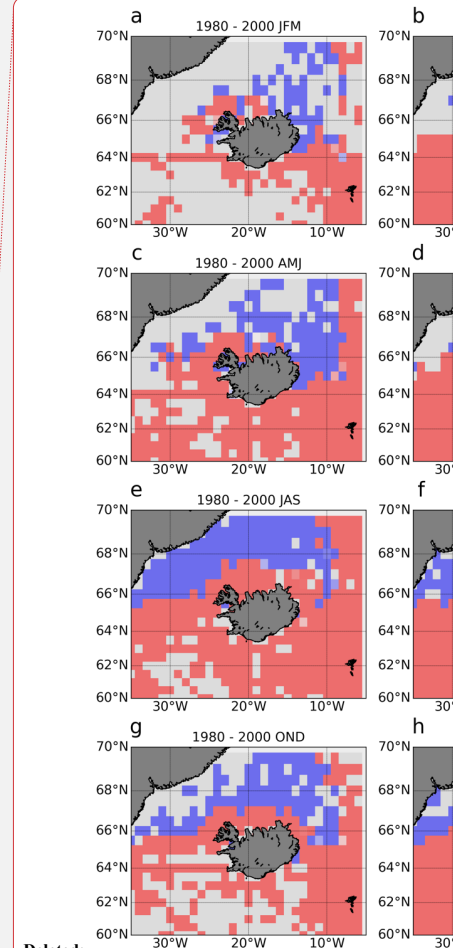


**Figure 8: Mean upper 200m spice frequency for the region of study showing the  $\alpha$ -ocean (red) and  $\beta$ -ocean (blue) regions for the periods of 1980-2000 and 2000-2020 and the four main seasons JFM (a,b), AMJ (c,d), JAS (e,f) and OND (g,h). The Brakstad et al (2023) hydrographic dataset is used for this calculation.**

The seasonal distribution of spice frequency north of Iceland agrees with the seasonal behavior of the NIIC described in Casanova-Masjoan et al. (2020) where the NIIC surface extension in winter and spring remains constrained to the northwestern side of Iceland due to the cold southeast surface imprint of the EIC. Then in summer, the NIIC expands northeastward, reaching all the way to the eastern side of Iceland and the northernmost station at the SI transect and constraining the polar water between the northern end of the Kolbeinsey Ridge and the Greenland shelf. Then in fall the NIIC northern extension narrows but is still able to surround Iceland. It is noteworthy that a clear increase in coverage of the  $\alpha$ -ocean, mainly in summer, is observed by comparing the 1980-200 average and the 2000-2010 average.

## 6. DISCUSSION AND CONCLUSIONS



Deleted:

Formatted: Font colour: Black

Formatted: Default Paragraph Font, Font colour: Black  
 Formatted: Normal, Centred, Border: Top: (No border), Bottom: (No border), Left: (No border), Right: (No border), Between : (No border), Tab stops: 7,96 cm, Centred + 15,92 cm, Right, Position: Horizontal: Left, Relative to: Column, Vertical: In line, Relative to: Margin, Wrap Around  
 Formatted: Font colour: Black

463 In this study, we discussed the seasonal and interannual variability of the mixed layer characteristics and the stratification  
464 regimes around Iceland by using a long **time series** of CTD data. Based on our results, we propose the regionalization of  
465 the waters around Iceland into three dynamical regions  $\alpha$ -ocean,  $\beta$ -ocean, and transition-ocean.

Deleted: timeseries

466 The southwestern region is dominated by AW both in winter and summer. Within this region, the winter MLD  
467 is the deepest and most variable of the whole study area, with ML's occupied by AW over the whole sampling period.  
468 This region is influenced by the dynamics of the Irminger Sea and the Subpolar gyre and has favorable conditions ( $\alpha$ -  
469 ocean) for winter deep convection driven by heat fluxes to develop deep mixed layers, which agrees with previous  
470 studies (Carmack, 2007; Våge et al., 2008; Piron et al., 2016; Stewart and Haine, 2016; Petit et al., 2020). In the  
471 Southern region, the ML salinity anomaly was negative over the last 5 years, which is consistent with previous  
472 numerical models and Argo observations showing a freshening trend of the North Atlantic (Tesdal et al., 2018;  
473 Holliday et al., 2020, Liu et al., 2020). However, since the South of Iceland is an  $\alpha$ -ocean, these recent changes have  
474 not **yet reached or affected** the MLD.

Formatted: Font: Cardo

475 The northwestern region, which includes the Denmark Strait, is a medley of all the water masses described in this study.  
476 In this region there is a confluence of Greenland shelf and slope waters and Iceland Sea origin waters (Harden et al., 2016;  
477 Foukal et al., 2020). This includes the NIIC generating an important variability in the water properties due to complex  
478 interactions of the regional currents (Lin et al. 2020, Mastropole et al. 2017). The MLD variability over time at the KG6  
479 and LB8 stations is moderate (<100m), except for the years 2000, 2007 and 2016 when the ML was anomalously deep. In  
480 this region, the stratification is notably year-round dominated by salinity ( $\beta$ -ocean), which is explained by the strong **Polar**  
481 influence of cold and fresh waters transported by the EGC. A broader look into the northwestern side of the basin reveals  
482 that this area can be divided at the center of the Denmark Strait into an  $\alpha$ -ocean near the Icelandic shelf where the NIIC  
483 flows and a  $\beta$ -ocean as we progress towards Greenland (where the LB8 and KG6 stations are located). Near the Icelandic  
484 shelf, MLDs are driven mainly by wind-stress, with a secondary contribution of heat fluxes. The T-S properties as well as  
485 the MLT anomalies in the northwest region near the Icelandic shelf show that the NIIC waters there are getting warmer and  
486 saltier. This agrees with previous studies showing the transformation of the NIIC also accompanied by an increase in its  
487 transport with time (Casanova-Masjoan et al., 2020). Even if the  $\alpha$ -ocean area is warming, it is not expanding  
488 northwestward. **Hence**, the EGC is acting as a barrier bringing PSW in the area and maintaining the  $\beta$ -ocean state on the  
489 northwesternmost side of the Strait.

Deleted: an effect

Formatted: Font: Cardo

Formatted: Font: Cardo

Deleted: Arctic

490 Northeast of Iceland, **the ML exhibits** intrusions of SW **in the winter, while AW is present during the summer**. In this  
491 region, the stratification changes from  $\beta$ - to  $\alpha$ -ocean seasonally. The Kolbeinsey Ridge acts as a barrier where we find the  
492 eastward penetration of the EIC bringing fresh waters (PSWw) from the East Greenland Current (Macrander et al., 2014;  
493 Casanova-Masjoan et al., 2020). In summer, the NIIC expands northeastward, bringing AW into the area and changing the  
494 stratification regime to  $\alpha$ . Hence, the mixed layer waters show important seasonal variability. **They** range from maximum  
495 temperature below 2 °C in winter to over 10 °C in summer. This is also the only region where a significant warming decadal  
496 trend emerges over the interannual variability and progressively results in a stronger  $\alpha$ -ocean. This agrees with the AW  
497 warming observed in Casanova-Masjoan et al. (2020) and with the northward progression of AW named as 'Atlantification'  
498 described by Polyakov et al. (2017). This shift to  $\alpha$ -ocean or 'Atlantification' may lead to deeper ML's (Moore et al., 2015;  
499 Våge et al., 2022), and the associated deeper convection may increase the potential of this area to contribute to the dense  
500 flow carried by the NIJ (Semper et al. 2019).

Deleted: , hence

Deleted: (and AW) have been detected

Deleted: (

Deleted: ) ML

Deleted: , they

501 The regionalization proposed in this work, based on hydrographic properties, matches the recently proposed distribution  
502 of primary production around Iceland (Richardson and Bendtsen, 2021; Cerfonteyn et al., 2023), supporting the importance

Formatted: Default Paragraph Font, Font colour: Black

Formatted: Normal, Centred, Border: Top: (No border), Bottom: (No border), Left: (No border), Right: (No border), Between : (No border), Tab stops: 7,96 cm, Centred + 15,92 cm, Right, Position: Horizontal: Left, Relative to: Column, Vertical: In line, Relative to: Margin, Wrap Around

Formatted: Font colour: Black

511 of MLD properties for the primary production (Ólafsson, 2003). The induced alterations on primary production can lead to  
512 ecosystem changes. For example, Iceland has witnessed a rapid increase in the population of mackerel, a relatively warm-  
513 water fish, since 2006 (Astthorsson et al., 2012; Campana et al., 2020) starting from the Southeast towards the north and  
514 recently they have been reported almost all around the country. This migration is consistent with our observations of both,  
515 the increase in surface temperatures, *i.e.*, northward shift of warmer isotherms over the Iceland Faroe Ridge (de Marez et  
516 al., 2025), and the increase of temperatures within the ML in the same regions over the last decade, which may establish  
517 new pathways for entire ecosystems.

518 The long time series investigated here revealed important interannual oscillations of the ML properties. Four main  
519 features are to be highlighted: (i) We do not observe any linear trend in the MLD, which is rather subjected to strong  
520 interannual variability (ii) Except for the southern stations, influenced by the subpolar gyre, the interannual variability was  
521 not correlated with the NAO. **For example, FX9 shows a significant negative of MLT with the NAO ( $R=-0.41$  and  $p\text{-value}$   
522  $< 0.03$ ).** (iii) The linear fit indicates significant (at 95%) warming trends in the MLT of most of the stations in winter, **with**  
523 **the maximum trend of  $0.08\text{ }^{\circ}\text{C}/\text{year}$  at S18 resulting in approximately  $2.2\text{ }^{\circ}\text{C}$ .** This agrees with previous studies (Sarafanov,  
524 2009) showing that the northern part of the North Atlantic (**South** of Iceland) is strongly dominated by atmospheric  
525 interannual to decadal variability, particularly, where AW is present. The exception here is the Northeastern region of  
526 Iceland where we observe a clear warming trend of the ML (2010-2020). (iv) We observe an ‘Atlantification’ expressed as  
527 a northeastward progression of the  $\alpha$ -ocean state. This progression will highlight the role of the northeastern area of Iceland  
528 as a convective zone where deep water could be formed and contribute to the NIJ.

Deleted: at times reaching

Deleted: south

## 529 AUTHOR CONTRIBUTIONS

530 Conceptualization, ARA, MDPH and EP; methodology, ARA, EP and MDPH; software, ARA and AP; formal analysis,  
531 ARA, EP, TM, CdM and MDPH; investigation, ARA, EP and MDPH, AM; data acquisition, SRÓ and AM; data curation,  
532 SRÓ and AM; writing—original draft preparation, ARA, EP and MDPH; writing—review and editing, SRÓ, AM and SJ,  
533 TM; visualization, ARA and EP; project administration, SRÓ; funding acquisition, ARA and SRÓ. All authors have read  
534 and agreed to the published version of the manuscript.

## 535 FUNDING

536 ARA has been supported by HM Queen Margrethe II’s and Vigdís Finnbogadóttir’s Interdisciplinary Research Centre on  
537 Ocean, Climate and Society (ROCS) under grant no. 158-4223. Support for this work was also provided by the European  
538 Union’s Horizon 2020 research and innovation programme under grant no. 727852, Blue-Action project (AM and SJ).  
539 This work has been supported by the FAR-DWO (PID2020-114322RBI00) project from the Spanish Ministry of  
540 Research.

## 541 ACKNOWLEDGMENTS

542 We are grateful for the invaluable cooperation we have had with the crews of the Icelandic research vessels Bjarni  
543 Sæmundsson and Árni Friðriksson and to the many people at the Marine Research Institute that have contributed to the  
544 hydrographic observations over the years. **ARA and MDPH would like to dedicate this paper to the memory of Maria**  
545 **Casanova-Masjoan.**

Formatted: Font: Arial, 11 pt

Formatted: Default Paragraph Font, Font colour: Black

Formatted: Normal, Centred, Border: Top: (No border),  
Bottom: (No border), Left: (No border), Right: (No border),  
Between : (No border), Tab stops: 7,96 cm, Centred + 15,92  
cm, Right, Position: Horizontal: Left, Relative to: Column,  
Vertical: In line, Relative to: Margin, Wrap Around

Formatted: Font colour: Black

549 **Table 1.** Characteristics for the representative stations for each typical surveyed section. The representative ocean currents  
 550 at each section are also shown: North Icelandic Irminger Current (NIIC), Irminger Current (IC), East Greenland Current  
 551 (EGC), North Icelandic Jet (NIJ), East Icelandic Current (EIC), and North Atlantic Current. (NAC).

552  
 553

Station	Depth, m	Lon	Lat	Oceanic region	Significant currents
Faxaflói (FX9)	1010	-27.98	64.35	Subpolar North Atlantic	IC
Látrabjarg (LB8)	658	-27.050	66.083	Denmark Strait	NIIC, EGC, DSO
Kögur (KG6)	980	-23.933	67.583	Western Iceland Sea	EGC, DSO
Hornbanki (HB6)	612	-21.583	67.50	Western Iceland Sea	NIIC, NIJ
Síglunes (S18)	1023	-18.83	68.00	Kolbeinsey Ridge	NIIC, EGC, EIC, NIJ
Langanes NE (LN6)	1850	-12.66	68.00	Iceland Sea	EIC
Langanes E (LA8)	1251	-9.00	66.37	Iceland Sea	EIC
Krossanes (KR6)	1419	-9.00	65.00	Iceland Sea/ North Atlantic	EIC, NAC
Stokksnes (ST5)	1153	-13.66	63.66	North Atlantic	NAC
Selvogsbanki (SB5)	1006	-21.48	62.98	North Atlantic	IC

Formatted Table

Deleted: Greenland

Deleted: Greenland

Formatted: Font colour: Auto

554  
 555  
 556  
 557

**Table 2.** Main water masses definitions for the region of study (Rudels et al., 2005; Våge et al., 2011)

Water mass	Potential Temperature ( $\theta$ )	Salinity	Potential density ( $\sigma_\theta$ , $\text{kg m}^{-3}$ )
Surface Water (SW)	$\geq 3^\circ\text{C}$	-	$\sigma_\theta < 27.70$
Warm Polar Surface Water (PSW <sub>w</sub> )	$0^\circ\text{C} \leq \theta < 3^\circ\text{C}$	-	$\sigma_\theta \leq 27$
Polar Surface Water (PSW)	$< 0^\circ\text{C}$ ,	-	$\sigma_\theta < 27.70$

Formatted Table

Deleted: -

Deleted: <

Deleted: <

Deleted:  $\geq$

Formatted: Default Paragraph Font, Font colour: Black

Formatted: Normal, Centred, Border: Top: (No border), Bottom: (No border), Left: (No border), Right: (No border), Between: (No border), Tab stops: 7.96 cm, Centred + 15.92 cm, Right, Position: Horizontal: Left, Relative to: Column, Vertical: In line, Relative to: Margin, Wrap Around

Formatted: Font colour: Black

Atlantic Water(AW)	$> 3^{\circ}C$	$> 34.9$	-
Atlantic-origin Overflow Water (AtOW)	$0^{\circ}C \leq \theta < 3^{\circ}C$	-	$\sigma_0 \geq 27.8,$ $\sigma_{0.5} < 30.44$
Polar intermediate Water (PIW)	$0^{\circ}C$	$\leq 34.676$	$\sigma_0 > 27.70,$
Arctic-origin Overflow Water (ArOW)	$< 0^{\circ}C$	-	$\sigma_0 > 27.8,$ $\sigma_{0.5} < 30.44$
Nordic Seas Deep Water (NDW)	$< 0^{\circ}C$	-	$\sigma_{0.5} \geq 30.44$

Deleted: <

Deleted: <

Formatted: Left

Deleted: ≤

Deleted: ≥

564  
565  
566  
567  
568  
569  
570  
571  
572  
573  
574  
575  
576  
577  
578  
579  
580  
581  
582  
583  
584

Formatted: Default Paragraph Font, Font colour: Black

Formatted: Normal, Centred, Border: Top: (No border), Bottom: (No border), Left: (No border), Right: (No border), Between : (No border), Tab stops: 7,96 cm, Centred + 15,92 cm, Right, Position: Horizontal: Left, Relative to: Column, Vertical: In line, Relative to: Margin, Wrap Around

Formatted: Font colour: Black

585

590 **References**

591 Asthorrsson, O. S., Valdimarsson, H., Gudmundsdottir, A., and Oskarsson, G. J.: Climate-related variations in the  
592 occurrence and distribution of mackerel (*Scomber scombrus*) in Icelandic waters, *ICES J. Mar. Sci.*, 69, 1289–1297, 2012.

593 Athanase, M., Provost, C., Perez-Hernández, M. D., Sennechael, N., Bertasio, C., Artana, C., et al.: Atlantic water  
594 modification north of Svalbard in the Mercator physical system from 2007 to 2020, *J. Geophys. Res.: Oceans*, 125,  
595 e2020JC016463, <https://doi.org/10.1029/2020JC016463>, 2020.

596 Bachman, S. D., Taylor, J., Adams, K., and Hosegood, P.: Mesoscale and submesoscale effects on mixed layer depth in  
597 the Southern Ocean, *J. Phys. Oceanogr.*, 47, 2173–2188, 2017.

598 Bindoff, N. L., Cheung, W. W., Kairo, J. G., Aristegui, J., Guinder, V. A., Hallberg, R., et al.: Changing ocean, marine  
599 ecosystems, and dependent communities, IPCC Special Report on the Ocean and Cryosphere in a Changing Climate, 477–  
600 587, 2019.

601 Brakstad, A.: Hydrographic and Geochemical Observations in the Nordic Seas Between 1950 and 2019, University of  
602 Bergen, 2023b.

603 Bersch, M.: North Atlantic Oscillation–induced changes of the upper layer circulation in the northern North Atlantic Ocean,  
604 *J. Geophys. Res.*, 107(C10), 3156, <https://doi.org/10.1029/2001JC000901>, 2002.

605 Campana, S. E., Stefansdottir, R. B., Jakobsdottir, K., and Solmundsson, J.: Shifting fish distributions in warming sub-  
606 Arctic oceans, *Sci. Rep.*, 10, 1–14, 2020.

607 Carmack, E. C.: The alpha/beta ocean distinction: A perspective on freshwater fluxes, convection, nutrients and  
608 productivity in high-latitude seas, *Deep Sea Res. Part II: Top. Stud. Oceanogr.*, 54, 2578–2598, 2007.

609 Carton, J. A., Grodsky, S. A., and Liu, H.: Variability of the oceanic mixed layer, 1960–2004, *J. Climate*, 21, 1029–1047,  
610 2008.

611 Casanova-Masjoan, M., Perez-Hernández, M. D., Pickart, R. S., Valdimarsson, H., Ólafsdóttir, S., Macrander, A., et al.:  
612 Along-stream, seasonal, and interannual variability of the North Icelandic Irminger Current and East Icelandic Current  
613 around Iceland, *J. Geophys. Res.: Oceans*, 125, e2020JC016283, <https://doi.org/10.1029/2020JC016283>, 2020.

614 Cerfonteyn, M., Groben, R., Vaulot, D., et al.: The distribution and diversity of eukaryotic phytoplankton in the Icelandic  
615 marine environment, *Sci. Rep.*, 13, 8519, <https://doi.org/10.1038/s41598-023-35516-w>, 2023.

616 Dai, A., Luo, D., Song, M., and Liu, J.: Arctic amplification is caused by sea-ice loss under increasing CO<sub>2</sub>, *Nat. Commun.*,  
617 10, 1–13, 2019.

618 de Boyer Montegut, C., Madec, G., Fischer, A. S., Lazar, A., and Iudicone, D.: Mixed layer depth over the global ocean:  
619 An examination of profile data and a profile-based climatology, *J. Geophys. Res.: Oceans*, 109,  
620 <https://doi.org/10.1029/2004JC002378>, 2004.

621 de Marez, C., Ruiz-Angulo, A., & Gula, J. ~~Mesoscale induced vertical fluxes over the Iceland-Faroe ridge. *Geophysical*~~  
622 ~~*Research Letters*, 52(13), 2025.~~

623 ~~Feucher, C., Portela, E., Kolodziejczyk, N., & Thierry, V. Subpolar gyre decadal variability explains the recent~~  
624 ~~oxygenation in the Irminger Sea. *Communications Earth & Environment*, 3(1), 279, 2022.~~

625 Foukal, N. P., Gelderloos, R., and Pickart, R. S.: A continuous pathway for fresh water along the east Greenland shelf, *Sci.*  
626 *Adv.*, 6, eabc4254, 2020.

- Deleted: -
- Deleted: and
- Deleted: : High-resolution characterization of mesoscale eddies and
- Deleted: heat
- Deleted: estimate atop
- Deleted:
- Deleted: Ridge, *Geophys. Res. Lett.*, submitted
- Formatted: Default Paragraph Font, Font colour: Black
- Formatted: Normal, Centred, Border: Top: (No border), Bottom: (No border), Left: (No border), Right: (No border), Between : (No border), Tab stops: 7.96 cm, Centred + 15.92 cm, Right, Position: Horizontal: Left, Relative to: Column, Vertical: In line, Relative to: Margin, Wrap Around
- Formatted: Font colour: Black

- 635 Hafrannsóknastofnun: Makrill *Scomber scombrus* Stofnmatskýrslur (stock assessment report), Hafrannsóknastofnun,  
636 2024, [https://www.hafogvatn.is/static/extras/images/mackerel\\_2024\\_techreport\\_is.html](https://www.hafogvatn.is/static/extras/images/mackerel_2024_techreport_is.html).
- 637
- 638 Hansen, B., and Østerhus, S.: North Atlantic–Nordic Seas exchanges, *Prog. Oceanogr.*, 45, 109–208, 2000.
- 639 Harden, B., Renfrew, I., and Petersen, G.: Meteorological buoy observations from the central Iceland Sea, *J. Geophys.*  
640 *Res.-Atmos.*, 120, 3199–3208, 2015.
- 641 Harden, B. E., Pickart, R. S., Valdimarsson, H., Vage, K., de Steur, L., Richards, C., et al.: Upstream sources of the  
642 Denmark Strait overflow: Observations from a high-resolution mooring array, *Deep-Sea Res. Pt. I*, 112, 94–112, 2016.
- 643 Hátún, H., and Chafik, L.: On the recent ambiguity of the North Atlantic Subpolar Gyre Index, *J. Geophys. Res.-Oceans*,  
644 123, 5072–5076, 2018.
- 645 Hátún, H., Chafik, L., and Larsen, K. M. H.: The Norwegian Sea Gyre – a regulator of Iceland-Scotland Ridge exchanges,  
646 *Front. Mar. Sci.*, 8, 1001, 2021.
- 647 Havik, L., Pickart, R. S., Våge, K., Torres, D. J., Thurnherr, A., Beszczynska-Möller, A., et al.: Evolution of the East  
648 Greenland Current from Fram Strait to Denmark Strait: Synoptic measurements from summer 2012, *J. Geophys. Res.-*  
649 *Oceans*, 122, 1974–1994, 2017.
- 650 Hersbach, H., Bell, B., Berrisford, P., et al.: The ERA5 global reanalysis, *Q. J. R. Meteorol. Soc.*, 146, 1999–2049,  
651 <https://doi.org/10.1002/qj.3803>, 2020.
- 652 Holt, J., Schrum, C., Cannaby, H., Daewel, U., Allen, I., Artioli, Y., et al.: Potential impacts of climate change on the  
653 primary production of regional seas: A comparative analysis of five European seas, *Prog. Oceanogr.*, 140, 91–115, 2016.
- 654 Holte, J., Talley, L. D., Gilson, J., and Roemmich, D.: An Argo mixed layer climatology and database, *Geophys. Res. Lett.*,  
655 44, 5618–5626, 2017.
- 656 Ingvaldsen, R. B., Assmann, K. M., Primicerio, R., Fosheim, M., Polyakov, I. V., and Dolgov, A. V.: Physical  
657 manifestations and ecological implications of Arctic Atlantification, *Nat. Rev. Earth Environ.*, 2, 874–889, 2021.
- 658 Jónsson, S.: The circulation in the northern part of the Denmark Strait and its variability, *ICES CM*, 50, 1999.
- 659 Jónsson, S., and Briem, J.: Flow of Atlantic water west of Iceland and onto the North Icelandic shelf, 2003.
- 660 Jónsson, S., and Valdimarsson, H.: Water mass transport variability to the North Icelandic shelf, 1994–2010, *ICES J. Mar.*  
661 *Sci.*, 69, 809–815, <https://doi.org/10.1093/icesjms/fss024>, 2012.
- 662 Kohler, J., Serra, N., Bryan, F. O., Johnson, B. K., and Stammer, D.: Mechanisms of mixed-layer salinity seasonal  
663 variability in the Indian Ocean, *J. Geophys. Res.-Oceans*, 123, 466–496, 2018.
- 664 Li, G., Cheng, L., Zhu, J., Trenberth, K. E., Mann, M. E., and Abraham, J. P.: Increasing ocean stratification over the past  
665 half-century, *Nat. Clim. Chang.*, 10, 1116–1123, 2020.
- 666 Liu, C., Liang, X., Chambers, D. P., and Ponte, R. M.: Global patterns of spatial and temporal variability in salinity from  
667 multiple gridded Argo products, *J. Clim.*, 33, 8751–8766, 2020.
- 668 Logemann, K., Ólafsson, J., Snorrason, A., Valdimarsson, H., and Marteinsdóttir, G.: The circulation of Icelandic waters  
669 – a modelling study, *Ocean Sci.*, 9, 931–955, 2013.
- 670 Lozier, M. S., Li, F., Bacon, S., Bahr, F., Bower, A. S., Cunningham, S., et al.: A sea change in our view of overturning in

**Formatted:** Default Paragraph Font, Font colour: Black

**Formatted:** Normal, Centred, Border: Top: (No border),  
Bottom: (No border), Left: (No border), Right: (No border),  
Between : (No border), Tab stops: 7,96 cm, Centred + 15,92  
cm, Right, Position: Horizontal: Left, Relative to: Column,  
Vertical: In line, Relative to: Margin, Wrap Around

**Formatted:** Font colour: Black

671 the subpolar North Atlantic, *Science*, 363, 516–521, 2019.

672 ~~Macrander, A., Valdimarsson, H., and Jonsson, S.: Improved transport estimate of the East Icelandic Current 2002–2012,~~  
673 ~~J. Geophys. Res.-Oceans, 119, 3407–3424, 2014.~~

674 Mastropole, D., Pickart, R. S., Valdimarsson, H., Våge, K., Jochumsen, K., and Girton, J.: On the hydrography of Denmark  
675 Strait, *J. Geophys. Res.-Oceans*, 122, 306–321, 2017.

676 Mauritzen, C.: Production of dense overflow waters feeding the North Atlantic across the Greenland-Scotland Ridge. Part  
677 1: Evidence for a revised circulation scheme, *Deep-Sea Res. Pt. I*, 43, 769–806, 1996.

678 [Moore, G. W. K., Våge, K., Pickart, R. S., & Renfrew, I. A. \(2015\). Decreasing intensity of open-ocean convection in the  
679 Greenland and Iceland seas. \*Nature Climate Change\*, 5\(9\), 877–882.](#)

680 Ólafsson, J.: Winter mixed layer nutrients in the Irminger and Iceland seas, *ICES Mar. Sci. Symp.*, 219, 329–332, 2003.

681 Intergovernmental Panel on Climate Change (IPCC): Special report on the ocean and cryosphere in a changing climate,  
682 2019.

683 Ólafsdóttir, A. H., Utne, K. R., Jacobsen, J. A., Jansen, T., Óskarsson, G. J., Nottestad, L., Elvarsson, B. Þ., Broms, C.,  
684 and Slotte, A.: Geographical expansion of Northeast Atlantic mackerel (*Scomber scombrus*) in the Nordic Seas from 2007  
685 to 2016 was primarily driven by stock size and constrained by low temperatures, *Deep-Sea Res. Pt. II*, 159, 152–168, 2019.

686 Østerhus, S., Woodgate, R., Valdimarsson, H., Turrell, B., De Steur, L., Quadfasel, D., Olsen, S. M., Moritz, M., Lee, C.  
687 M., Larsen, K. M. H., and Jónsson, S.: Arctic Mediterranean exchanges: a consistent volume budget and trends in transports  
688 from two decades of observations, *Ocean Sci.*, 15, 379–399, 2019.

689 Perez, F. F., Ólafsson, J., Olafsdóttir, S. R., Fontela, M., and Takahashi, T.: Contrasting drivers and trends of ocean  
690 acidification in the subarctic Atlantic, *Sci. Rep.*, 11, 1–16, 2021.

691 Perez-Hernández, M. D., Pickart, R. S., Torres, D. J., Bahr, F., Sundfjord, A., Ingvaldsen, R., et al.: Structure, transport,  
692 and seasonality of the Atlantic Water boundary current north of Svalbard: Results from a yearlong mooring array, *J.*  
693 *Geophys. Res.-Oceans*, 124, 1679–1698, 2019.

694 Petit, T., Lozier, M. S., Josey, S. A., and Cunningham, S. A.: Atlantic deep water formation occurs primarily in the Iceland  
695 Basin and Irminger Sea by local buoyancy forcing, *Geophys. Res. Lett.*, 47, e2020GL091028, 2020.

696 Petit, T., Lozier, M. S., Josey, S. A., and Cunningham, S. A.: Role of air-sea fluxes and ocean surface density on the  
697 production of deep waters in the eastern subpolar gyre of the North Atlantic, *Ocean Sci. Discuss.*, 1–21, 2021.

698 Piron, A., Thierry, V., Mercier, H., and Caniaux, G.: Argo float observations of basin-scale deep convection in the Irminger  
699 Sea during winter 2011–2012, *Deep-Sea Res. Pt. I*, 109, 76–90, 2016.

700 Polyakov, I. V., Pnyushkov, A. V., Alkire, M. B., Ashik, I. M., Baumann, T. M., Carmack, E. C., et al.: Greater role for  
701 Atlantic inflows on sea-ice loss in the Eurasian Basin of the Arctic Ocean, *Science*, 356, 285–291, 2017.

702 Polyakov, I. V., Rippeth, T. P., Fer, I., Alkire, M. B., Baumann, T. M., Carmack, E. C., et al.: Weakening of cold halocline  
703 layer exposes sea ice to oceanic heat in the eastern Arctic Ocean, *J. Clim.*, 33, 8107–8123, 2020.

704 Price, J. F., Weller, R. A., and Pinkel, R.: Diurnal cycling – Observations and models of the upper ocean response to diurnal  
705 heating, cooling, and wind mixing, *J. Geophys. Res.-Oceans*, 91, 8411–8427, 1986.

706 Renfrew, I. A., Pickart, R. S., Våge, K., Moore, G. W., Bracegirdle, T. J., Elvidge, A. D., et al.: The Iceland Greenland  
707 Seas Project, *Bull. Am. Meteorol. Soc.*, 100, 1795–1817, 2019.

Deleted: ¶

Formatted: Default Paragraph Font, Font colour: Black

Formatted: Normal, Centred, Border: Top: (No border),  
Bottom: (No border), Left: (No border), Right: (No border),  
Between : (No border), Tab stops: 7,96 cm, Centred + 15,92  
cm, Right, Position: Horizontal: Left, Relative to: Column,  
Vertical: In line, Relative to: Margin, Wrap Around

Formatted: Font colour: Black

709 Reynolds, R. and Banzon, V.: NOAA optimum interpolation 1/4 degree daily sea surface temperature (OISST) analysis,  
710 version 2, NOAA Natl. Cent. Environ. Inf., 10, V5SQ8XB5, 2008.

711 Richardson, K. and Bendtsen, J.: Distinct seasonal primary production patterns in the sub-polar gyre and surrounding seas,  
712 Front. Mar. Sci., 2021.

713 Rudels, B., Björk, G., Nilsson, J., Winsor, P., Lake, I., and Nohr, C.: The interaction between waters from the Arctic Ocean  
714 and the Nordic Seas north of Fram Strait and along the East Greenland Current: Results from the Arctic Ocean-02 Oden  
715 expedition, J. Mar. Syst., 55, 1–30, 2005.

716 Sallée, J.-B., Pellichero, V., Akhoudas, C., Pauthenet, E., Vignes, L., Schmidtko, S., et al.: Summertime increases in upper-  
717 ocean stratification and mixed-layer depth, Nature, 591, 592–598, 2021.

718 Sarafanov, A.: On the effect of the North Atlantic Oscillation on temperature and salinity of the subpolar North Atlantic  
719 intermediate and deep waters, ICES J. Mar. Sci., 66, 1448–1454, 2009.

720 Sarmiento, J. L., Hughes, T. M., Stouffer, R. J., and Manabe, S.: Simulated response of the ocean carbon cycle to  
721 anthropogenic climate warming, Nature, 393, 245–249, 1998.

722 Semper, S., Våge, K., Pickart, R. S., Valdimarsson, H., Torres, D. J., and Jónsson, S.: The emergence of the North Icelandic  
723 Jet and its evolution from Northeast Iceland to Denmark Strait, J. Phys. Oceanogr., 49, 2499–2521, 2019.

724 Shepherd, J. G., Brewer, P. G., Oschlies, A., and Watson, A. J.: Ocean ventilation and deoxygenation in a warming world:  
725 Introduction and overview, 2017 [Dataset].

726 Skillingstad, E. D., Samelson, R. M., Simmons, H., Laurent, L. S., Merrifield, S., Klenz, T., and Centurioni, L.: Boundary  
727 layer energetics of rapid wind and wave forced mixing events, J. Phys. Oceanogr., 53, 1887–1900, 2023.

728 Stewart, K. D. and Haine, T. W.: Thermobaricity in the transition zones between alpha and beta oceans, J. Phys. Oceanogr.,  
729 46, 1805–1821, 2016.

730 Strehl, A.-M., Våge, K., Merdrud, S. L. H., and Barreyre, T.: A 70-year perspective on water-mass transformation in the  
731 Greenland Sea: From thermobaric to thermal convection, Prog. Oceanogr., 227, 103304, 2024.

732 Swift, J. H., Aagaard, K., and Malmberg, S.-A.: The contribution of the Denmark Strait overflow to the deep North Atlantic,  
733 Deep-Sea Res. Pt. A, 27, 29–42, 1980.

734 Tesdal, J.-E., Abernathy, R. P., Goes, J. I., Gordon, A. L., and Haine, T. W.: Salinity trends within the upper layers of the  
735 subpolar North Atlantic, J. Clim., 31, 2675–2698, 2018.

736 Valdimarsson, H., Astthórsson, O. S., and Pálsson, J.: Hydrographic variability in Icelandic waters during recent decades  
737 and related changes in distribution of some fish species, ICES J. Mar. Sci., 69, 816–  
738 825, <https://doi.org/10.1093/icesjms/fss027>, 2012.

739 Våge, K., Moore, G. W. K., Jónsson, S., and Valdimarsson, H.: Water mass transformation in the Iceland Sea, Deep-Sea  
740 Res. Pt. I, 101, 98–109, 2015.

741 Våge, K., Papritz, L., Havik, L., Spall, M. A., and Moore, G. W. K.: Ocean convection linked to the recent ice edge retreat  
742 along East Greenland, Nat. Commun., 9, 1–8, 2018.

743 Våge, K., Pickart, R. S., Moore, G., and Ribergaard, M. H.: Winter mixed layer development in the central Irminger Sea:  
744 The effect of strong, intermittent wind events, J. Phys. Oceanogr., 38, 541–565, 2008.

745 Våge, K., Pickart, R. S., Spall, M. A., Moore, G., Valdimarsson, H., Torres, D. J., et al.: Revised circulation scheme north

Deleted: ¶

Deleted: ¶

Formatted: Default Paragraph Font, Font colour: Black

Formatted: Normal, Centred, Border: Top: (No border), Bottom: (No border), Left: (No border), Right: (No border), Between : (No border), Tab stops: 7,96 cm, Centred + 15,92 cm, Right, Position: Horizontal: Left, Relative to: Column, Vertical: In line, Relative to: Margin, Wrap Around

Formatted: Font colour: Black

750 of the Denmark Strait, Deep-Sea Res. Pt. I, 79, 20–39, 2013.

751 Våge, K., Pickart, R. S., Spall, M. A., Valdimarsson, H., Jónsson, S., Torres, D. J., et al.: Significant role of the North  
752 Icelandic Jet in the formation of Denmark Strait Overflow Water, Nat. Geosci., 4, 723–727, 2011.

753 [Våge, K., Semper, S., Valdimarsson, H., Jónsson, S., Pickart, R. S., & Moore, G. W. K. \(2022\). Water mass transformation  
754 in the Iceland Sea: Contrasting two winters separated by four decades. Deep Sea Research Part I: Oceanographic Research  
755 Papers, 186, 103824.](#)

756 [Whitney, M. M. \(2025\). Icelandic riverine freshwater distribution, offshore export, and alongshelf connectivity. Estuarine,  
757 Coastal and Shelf Science, 319, 109266.](#)

758 Yamaguchi, R. and Suga, T.: Trend and variability in global upper-ocean stratification since the 1960s, J. Geophys. Res.-  
759 Oceans, 124, 8933–8948, 2019.

760

Deleted:

761

Formatted: Default Paragraph Font, Font colour: Black

Formatted: Normal, Centred, Border: Top: (No border), Bottom: (No border), Left: (No border), Right: (No border), Between : (No border), Tab stops: 7,96 cm, Centred + 15,92 cm, Right, Position: Horizontal: Left, Relative to: Column, Vertical: In line, Relative to: Margin, Wrap Around

Formatted: Font colour: Black